ISABE2015-20163

Complementary Aerodynamic Performance Datasets for Variable Speed Power Turbine Blade Section from Two Independent Transonic Turbine Cascades

Ashlie B. Flegel and Gerard E. Welch
NASA John H. Glenn Research Center at Lewis Field,
Cleveland, OH USA

Paul W. Giel
Vantage Partners LLC.
Cleveland, OH USA

Forrest E. Ames and Jonathan A. Long
University of North Dakota
Grand Forks, ND USA

Abstract

Two independent experimental studies were conducted in linear cascades on a scaled, two-dimensional midspan section of a representative Variable Speed Power Turbine (VSPT) blade. The purpose of these studies was to assess the aerodynamic performance of the VSPT blade over large Reynolds number and incidence angle ranges. The influence of inlet turbulence intensity was also investigated. The tests were carried out in the NASA Glenn Research Center Transonic Turbine Blade Cascade Facility and at the University of North Dakota (UND) High Speed Compressible Flow Wind Tunnel Facility. A large database was developed by acquiring total pressure and exit angle surveys and blade loading data for ten incidence angles ranging from +15.8° to −51.0°. Data were acquired over six flow conditions with exit isentropic Reynolds number ranging from 0.05×10^6 to 2.12×10^6 and at exit Mach numbers of 0.72 (design) and 0.35. Flow conditions were examined within the respective facility constraints. The survey data were integrated to determine average exit total-pressure and flow angle. UND also acquired blade surface heat transfer data at two flow conditions across the entire incidence angle range aimed at quantifying transitional flow behavior on the blade. Comparisons of the aerodynamic datasets were made for three "match point" conditions. The blade loading data at the match point conditions show good agreement between the facilities. This report shows comparisons of other data and highlights the unique contributions of the two facilities. The datasets are being used to advance understanding of the aerodynamic challenges associated with maintaining efficient power turbine operation over a wide shaft-speed range.

Nomenclature

Cp_s = static pressure coefficient, $Cp_s = \left(P - \bar{P}_2\right) / \left(P_{t,1} - \bar{P}_2\right)$
Cp_t = total pressure coefficient, $Cp_t = \left(P_{t,1} - P_t\right) / \left(P_{t,1} - \bar{P}_2\right)$
C_x = blade axial chord [in]
H = blade span [in]
i = incidence angle, $i = \beta_1 - 34.2°$
M = Mach number
$\bar{P}$ = area-averaged static-pressure
$\bar{P}_t$ = area-averaged total-pressure
Re = exit Reynolds number, $Re = \rho_{2,i} U_{2,i} C_x / \mu_2$
Re_b = baseline Reynolds number, $Re_b = 5.30\times10^5$
S = blade pitch [in]
SS = suction surface
Tu = turbulence intensity, $Tu = \sqrt{\overline{u^2}} / U$
$\underline{u}$ = fluctuating velocity
U = total mean velocity
x = chordwise (axial) coordinate [in]
y = pitchwise (tangential) coordinate [in]
z = spanwise coordinate [in]
Zw = Zweifel coefficient, $Zw = \frac{2S}{C_x}\cos^2\bar{\beta}_2(\tan\beta_1 - \tan\bar{\beta}_2)$
β = pitch angle [deg.], $\beta = \tan^{-1}(U_y / U_x)$
γ = yaw angle [deg.], $\gamma = \tan^{-1}(U_z / U_x)$
δ_{99} = endwall boundary layer thickness [in]
μ = dynamic viscosity
ρ = density
ω = loss coefficient, $\omega = \left(P_{t,1} - \bar{P}_t\right) / \left(P_{t,1} - \bar{P}_2\right)$
Ω = cross-passage loss coefficient, $(P_{t,1} - P_{t,2}) / (P_{t,1} - P_2)$

Subscripts
1 = cascade inlet value
2 = cascade exit value
i = isentropic value
s = streamwise component
t = total condition

Introduction

Variable-speed capability is a key enabling technology of next generation rotorcraft in both the commercial[1,2] and military[3] sectors. Taking advantage of the VTOL and high-speed cruise capability of rotorcraft, like the Large Civil Tilt Rotor (LCTR), would help reduce airport congestion and increase airspace throughput capacity. System studies have shown that in order to maintain the propulsive efficiency, the main rotor speeds must vary from 100% speed at take-off to 54% speed at cruise.[4] A Variable-Speed Power Turbine (VSPT) is one approach to handle this speed variation. The key aerodynamic challenges of the VSPT, due to this speed change, include attaining high turbine efficiency at high work factors, managing the loss levels over a large (40° to 60°) incidence variation, and operating at low cruise unit Reynolds numbers ($0.45\times10^5 < Re/C_x$ [in^{-1}] < 0.75×10^5) with transitional flow.[5,6]

Research is being conducted at the NASA Glenn Research Center using both experimental[7,8] and computational[9,10,11] methods to understand the aerodynamic challenges of a VSPT. Two datasets were developed in the NASA Glenn Transonic Turbine Cascade facility.[7,8] These datasets documented the aerodynamic effects over large incidence (+15.8° to −51.0°) and Reynolds number (2.12×10^5 to 2.12×10^6) ranges on a notional VSPT blade geometry.[12] NASA's facility, originally designed for testing at relevant high-pressure-turbine Mach and Reynolds numbers, was restricted on the minimum attainable Reynolds number. Consequently, the NASA testing was initially conducted at low turbulence intensity[7] (0.25% to 0.40%) with the intent that transitional flow, as expected at applicable (higher) turbulence intensities but at lower application Reynolds numbers, would be admitted. The low turbulence NASA experiments were then repeated at higher (engine relevant) turbulence levels[8] (8% to 15%). Accurate prediction of the influence of turbulence intensity with regions of laminar separation and transitional reattachment on both pressure- and suction-sides of the blading have already proven to be challenging for RANS CFD with transitional flow submodels.[11]

Heat transfer and aerodynamic studies were recently conducted at the University of North Dakota High Speed Compressible Flow Wind Tunnel Facility[13] on the same VSPT blade geometry.[14,15] The tunnel is a smaller scale and had the operational capability and test article size to enable attainment of the low (cruise altitude) Reynolds numbers while at the engine design exit Mach number. The UND tunnel and piping were modified as necessary to repeat eight discrete incidence angles of the NASA test ranging from +5.8° to −51.0° over Reynolds numbers of 0.45×10^5 to 5.3×10^5. Data were acquired at both low and high ($Tu \cong 0.4\%$ and 4.0%) turbulence intensities. The intent was to extend the NASA measurements to lower Reynolds numbers documenting effects on loading, transition, and separation.

This paper will discuss the complementary datasets and compare selected results from the facilities. Data from each facility were obtained at a mutually agreed "match point" condition ($Re_{Cx,2}$ = 530,000, $M_{2,i}$ = 0.72).

NASA's larger scale cascade allows for more detailed measurements, but limits the low Reynolds number range. The turbulence grid of that facility is also configured to generate higher levels and length scales of inlet turbulence. The smaller scale of the UND facility allowed for lower, altitude-cruise Reynolds numbers. The combination of the facilities' capabilities gives a very wide range of flow parameters applicable to future turbine development.

Facility Descriptions

NASA Transonic Turbine Blade Cascade Facility

The NASA Turbine Blade Cascade Facility, shown in Fig. 1, is a large-scale cascade comprising nominally ten blade passages. The operating envelope shown in Fig. 2 demonstrates the large independent range of engine-relevant Reynolds and Mach numbers within the facility's capability. More details of the facility can be found in the following references.[16, 17]

The blade cascade is mounted on a disk that can be rotated to provide an inlet flow angle range of $-17° \le \beta_1 \le +78.8°$ (from axial). Unique upper flow board extensions with respective blade suction-side profiling were installed, replacing the first blade, for five incidence angles in the range of $-16.1° \le i \le -51.0°$. Measurements were acquired for ten incidence angles ranging from $-17° \le \beta_1 \le +50°$ listed in Table 1. Detailed flowfield measurements were also obtained at the mission cruise (i = +5.8°) and takeoff (i = −36.7°) angles.

At each incidence angle, data were acquired at five flow conditions. These conditions are represented as pink triangles in Fig. 2 and are listed in Table 2. The baseline Reynolds number was determined as the lowest obtainable Reynolds condition the facility could achieve at the design exit Mach number of 0.72; this baseline Reynolds number of 530,000 was also a match point for the NASA and UND facilities. In the NASA cascade, $M_{2,i}$ = 0.35 data were also acquired in order to achieve a full order-of-magnitude variation in Reynolds number. This lower Reynolds number

($Re_{Cx,2}$ = 212,000, $M_{2,i}$ = 0.35) case provided another facility match point condition.

Testing was conducted at both low and high inlet turbulence intensity conditions. For the high inlet turbulence tests, an upstream blowing turbulence grid was installed roughly five-axial chords upstream of the center blade row leading edge. Figure 1 illustrates the turbulence grid, which is made up of one vertical one-inch square tube spanning the upper and lower inlet boards and five or six horizontal one-inch square tubes. Turbulence intensities were measured (and integral length scales determined) 0.415·C_x upstream of the blade row by Thurman et al.[18] for the high (Tu = 8%-15%) and low turbulence (Tu = 0.25%-0.40%) cases.

UND High Speed Compressible Flow Wind Tunnel Facility

The UND Compressible Flow Cascade Facility is shown schematically in Fig. 3. The closed-loop tunnel is driven by a Roots™ blower, which has an inlet volumetric flow rate of 1.89 m^3/s. The tunnel achieves independent control of Mach number by driving the blower with a variable frequency drive. The Reynolds number is changed by varying the pressure within the closed loop tunnel. The blade cascade used for the current experiment was configured in a 6 blade, 5-passage arrangement as shown in Fig. 4. The variation in inlet angle from +40° to −17° was achieved using 8 angled inlet nozzles along with 8 sets of matching inlet bleed flow blocks. A list of the inlet angles is given in Table 1. The present tests were run at inlet total pressures ranging from around 66 kPa to below 6 kPa for the design Mach number cases to produce axial chord exit Reynolds numbers ranging from 530,000 to 46,000. These conditions are listed in Table 3. The facility can produce either a low turbulence condition ($Tu \cong$ 0.4%) or a higher turbulence condition ($Tu \cong$ 4.0%) by using a smooth nozzle or a mock aero-combustor turbulence generator upstream of the angled nozzle. The facility is described in more detail in the following references.[13-15]

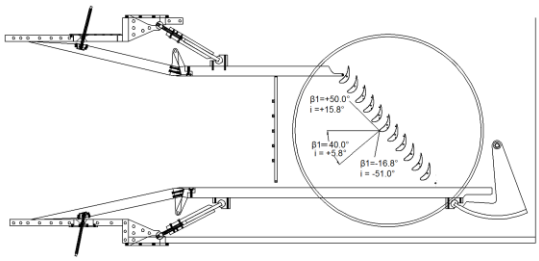

Figure 1. NASA Transonic Turbine Blade Cascade Facility

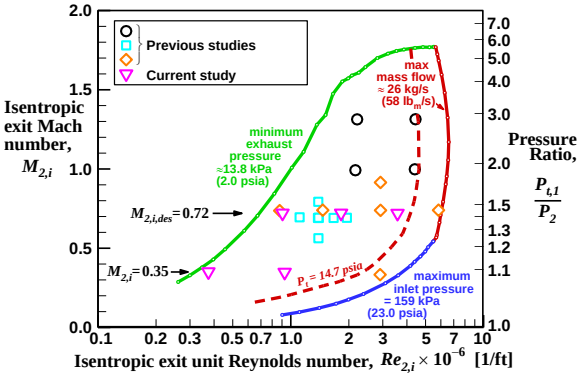

Figure 2. NASA CW-22 Operating Envelope.

Table 1. Inlet Flow Angles.

Inlet Angle, β_1	i	Zw	Facility
50.0°	15.8°	1.22	NASA
45.0°	10.8°	1.13	NASA
40.0° (Cruise)	5.8°	1.06	both
34.2°	0.0°	0.99	both
28.0°	−6.2°	0.92	both
18.1°	−16.1°	0.82	both
8.2°	−26.0°	0.74	both
−2.5° (Takeoff)	−36.7°	0.65	both
−11.8° (Mission Max-i)	−46.0°	0.58	both
−16.8°	−51.0°	0.53	both

Table 2. NASA CW-22 Nominal Flow Conditions

Flow Parameters		
Exit Re_{Cx}	Pressure Ratio	Exit M_{is}
2.12 × 10^6 (4.0·Re_b)	1.412	0.72
1.06 × 10^6 (2.0·Re_b)	1.412	0.72
5.30 × 10^5 (1.0·Re_b)	1.412	0.72
5.30 × 10^5 (1.0·Re_b)	1.087	0.35
2.12 × 10^5 (0.4·Re_b)	1.087	0.35

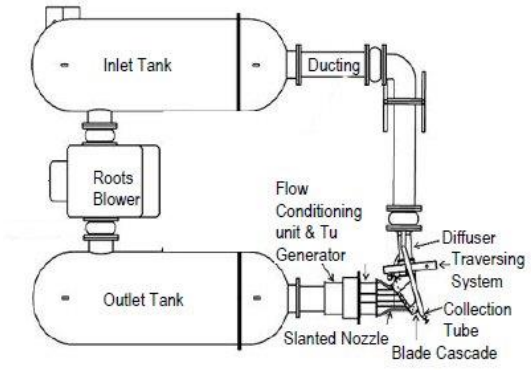

Figure 3. UND Compressible flow facility showing high turbulence configuration with 40° inlet angle.

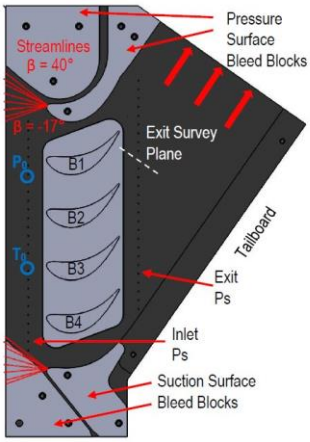

Figure 4. Schematic of UND linear blade cascade.

Table 3. UND Nominal Cascade Flow Conditions

Flow Parameters		
Exit Re_{Cx}	Pressure Ratio	Exit M_{is}
5.27×10^5 ($1.00 \cdot Re_b$)	1.412	0.72
2.12×10^5 ($0.40 \cdot Re_b$)	1.412	0.72
6.12×10^4 ($0.12 \cdot Re_b$)	1.412	0.72
4.64×10^4 ($0.09 \cdot Re_b$)	1.412	0.72
5.27×10^5 ($1.00 \cdot Re_b$)	1.087	0.35
2.12×10^5 ($0.40 \cdot Re_b$)	1.087	0.35

Blade Description

The blade geometry, shown in Fig. 5, is a scaled-up 2-D midspan section of a second-stage rotor of a 4-stage VSPT conceptual design.[12] Details of the blade and the design/ optimization process used to establish the 2-D profile are documented by Ford et al.[12] The details of the test blades for both facilities are listed in Table 4.

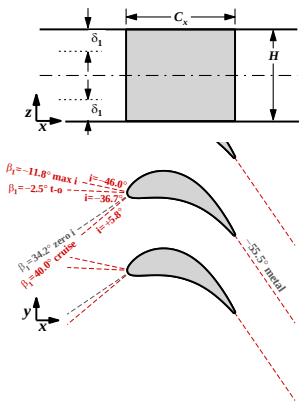

Figure 5. VSPT Blade Profile.

Table 4 Blade Description

Parameter	NASA Value	UND Value
Axial Chord, C_x [inch]	7.109	2.673
True Chord [inch]	7.655	2.878
Pitch, S [inch]	5.119	1.925
Span, H [inch]	6.000	2.000
Solidity, C_x/S	1.389	1.388
Aspect Ratio, H/C_x	0.844	0.748
Throat Dimension [inch]	2.868	1.062
Stagger Angle [deg.]	20.35°	20.35°
Inlet Metal Angle [deg.]	34.2°	34.2°
Uncovered Turning deg.]	19.47°	19.47°
Exit Metal Angle [deg.]	−55.54°	−55.54°

Measurement Description

NASA Transonic Turbine Blade Cascade Facility

Total-pressure, exit flow angle, and surface static pressure measurements acquired in the NASA facility are concentrated around the central-most blades. In Fig. 6, the locations of the upstream and downstream survey planes used in this study are shown. Total-pressure and exit flow angle data were acquired using a three-hole boundary layer probe and a five-hole pitch-yaw probe described in references[7,8]. Downstream measurements were obtained at the Station 2 location which is roughly 7.0% axial-chord downstream of the blade trailing edge and covers three blade passages.

Inlet boundary-layer measurements were made at the Station 0 location for two incidence angles (i = +5.8° and –36.7°) at the five flow conditions. The inlet boundary layer thickness, $\delta_{99,1}$, was correlated to the inlet Reynolds number. The inlet boundary layer thickness ranges are listed in Table 5. The turbulence grid reduced $\delta_{99,1}$ by a factor of two, but still covered 20%-30% of the blade span.

The primary measurement blades 4, 5, and 6, shown in Fig. 6, were instrumented with static pressure taps at four spanwise (10%, 15%, 30%, and 50%) locations. Additional facility measurements used to set Reynolds and Mach number conditions are discussed in the following references.[7,8]

UND High Speed Compressible Flow Wind Tunnel Facility

Measurements acquired in the Compressible Flow Rig at UND include midspan pressure distributions on Blades 2 and 3, midspan heat transfer measurements on Blade 2, and exit loss surveys acquired downstream of Blade 2 (see Fig. 4). Blade 2 loading distributions were acquired using 36 midspan pressure taps. Blade 3 had 18 taps at midspan and 18 taps at 25% span in alternating positions. A 5-element inlet boundary layer

rake was integrated into each inlet Kiel and total temperature probe. Readings from these two probes on each side of Blade 2 were analyzed to estimate inlet boundary layer information, which is reported in Table 6 for both high and low turbulence levels. Additional inlet and exit measurements are discussed elsewhere.[14,15]

Heat transfer measurements were acquired using the constant heat flux method. Heated and adiabatic wall surface temperatures at midspan were determined using temperature data from 36 fine wire thermocouples combined with finite difference analyses to account for conduction effects. The foil heater bus bars were integrated into the trailing edge.

Constant temperature hot wire anemometry measurements were acquired in UND's CFR facility to quantify the turbulence and unsteadiness for the low and aero-combustor turbulence conditions. The measurements were made using a single wire probe at the inlet of the previous vane cascade[13]. Turbulence values were estimated to range from 3.4% to 4.5% for the aero-combustor condition and 0.32% to 0.42% for the low turbulence condition depending on inlet angle. Additionally, shaft-order unsteadiness caused by the Roots blower was observed at four times its rotational rate. The rms unsteadiness was estimated to range from 0.5% to 0.7% and was present in the low turbulence condition.

Half-span exit traverses were made downstream of Blade 2 from the center of the passage between Blades 2 and 3 to the center of the passage between Blades 1 and 2. The traverse was made normal to the flow as shown in Fig. 4 with a 0.125 in diameter five-hole cone probe. The probe crossed the plane of the exit static pressures at approximately one-quarter axial chord downstream from the blade trailing edge plane. The full surveys included 21 locations in the spanwise direction and 21 locations in the cross-passage direction. The five-hole cone probe was calibrated as a function of angle, Mach number, and static pressure prior to the exit loss measurements.

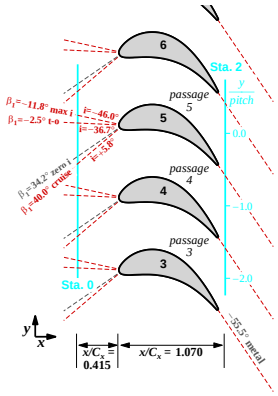

Figure 6. NASA Probe Survey Locations.

Table 5. NASA Inlet Endwall Boundary-Layer Thickness

Flow Parameter		Low Tu_1	
Exit Re_{Cx}	Exit M_{is}	$\delta_{99,1}$ † [in.]	$2\delta_{99,1}/H$ †
$4.0{\cdot}Re_b$	0.72	1.16 - 1.23	0.39 - 0.41
$2.0{\cdot}Re_b$	0.72	1.28 - 1.36	0.43 - 0.45
$1.0{\cdot}Re_b$	0.72	1.42 - 1.50	0.47 - 0.50
$1.0{\cdot}Re_b$	0.35	1.40 - 1.49	0.47 - 0.50
$0.4{\cdot}Re_b$	0.35	1.60 - 1.69	0.53 - 0.56
Flow Parameter		High Tu_1	
Exit Re_{Cx}	Exit M_{is}	$\delta_{99,1}$ † [in.]	$2\delta_{99,1}/H$ †
$4.0{\cdot}Re_b$	0.72	0.58 - 0.62	0.19 - 0.21
$2.0{\cdot}Re_b$	0.72	0.64 - 0.69	0.21 - 0.23
$1.0{\cdot}Re_b$	0.72	0.71 - 0.76	0.24 - 0.25
$1.0{\cdot}Re_b$	0.35	0.71 - 0.75	0.24 - 0.25
$0.4{\cdot}Re_b$	0.35	0.81 - 0.86	0.27 – 0.29

† Reynolds-scaling estimated range of endwall boundary-layer thickness at cascade inlet over ten incidence angle settings.

Table 6. UND Cascade Inlet Boundary Layers

		Low Turbulence				High Turbulence			
5.8°		46.4k	61.2k	212k	527k	46.4k	61.2k	212k	527k
	$C_f/2$	0.0032	0.0026	0.0036	0.0030	0.0038	0.0031	0.0034	0.0027
	θ (in)	0.0081	0.0070	0.0052	0.0033	0.0080	0.0066	0.0096	0.0106
	Re_θ	90.1	108.9	253	413	87.9	99.1	444	1,229
	H	2.41	2.43	1.63	1.54	2.37	2.36	1.47	1.35
-36.8	$C_f/2$	0.0039	0.0039	0.0042	0.0035	0.0036	0.0034	0.0037	0.0029
	θ (in)	0.0096	0.0085	0.0065	0.0051	0.0097	0.0082	0.0092	0.0093
	Re_θ	82.1	92.9	223	435	85.1	95.2	303	776
	H	2.36	2.39	1.62	1.45	2.40	2.41	1.53	1.39
-46°	$C_f/2$	0.0044	0.0036	0.0039	0.0029	0.0048	0.0039	0.0037	0.0029
	θ (in)	0.0096	0.0081	0.0056	0.0093	0.0094	0.0081	0.0094	0.0090
	Re_θ	77.2	92.1	191	749	78.9	92.1	313	750
	H	2.36	2.36	1.71	1.39	2.35	2.36	1.52	1.39

Note: This table refers to H as shape factor.

Results

Blade Loading

Comparisons of the two cascade facilities can first be made by observing the blade loading. Two match point conditions at both high and low turbulence are shown in Figs. 7 and 8 (i = +5.8°) and Fig. 9 (i = −51°).

The blade loading at the design point mission cruise condition with i = +5.8° is shown in Fig. 7. The UND cascade shows higher Cp_s on the suction side leading edge of the blade for each flow condition and turbulence level. This increased loading is attributed to the differences in inlet boundary layers. UND data not described in this paper show the inlet Mach number to be lower than the NASA cascade data. The thicker inlet boundary layers of the NASA cascade causes slightly higher inlet blockage resulting in

higher front end loading. Figure 7c shows the UND and NASA match-point data ($Re_{Cx,2}$ = 1×Re_b, $M_{2,i}$ = 0.72) at both high and low *Tu* compared to the design intent blade loading. The design calculation of Ford et al.[12] was carried out on a two-dimensional cone assuming fully turbulent flow. A laminar separation and reattachment is evident on the suction-side of the blades in the low *Tu* NASA data, even at this relatively high Reynolds number. The UND and NASA high *Tu* data are in substantial agreement and reflect fully attached, turbulent flow throughout the blade suction-side.

In Fig. 8 the effect of Reynolds number at i = +5.8° at low *Tu* is examined. This condition was chosen as there are notable transitional flow effects that can be observed on the trailing edge suction surface of the blade. In Fig. 8, separation is first indicated for 2×Re_b at roughly x/C_x = 0.76. For the design exit Mach number flow conditions, as Reynolds number decreases the reattachment point moves aft on the blade. This is depicted by the vertical lines shown in Figure 8. As the Mach number decreases to 0.35, the loading increases and separation is still observed. It is noted that the Reynolds number has minimal effect on the loading at the reduced Mach number.

At the most negative incidence angle, i = –51°, and at low inlet *Tu*, the NASA facility showed a leading edge pressure-side cove separation evident in Fig. 9a for 0.0 < x/C_x < 0.1, even at the highest Reynolds number. The low *Tu* UND data showed similar behavior[15]. However, at high *Tu*, flow in this region remained attached, despite the strong deceleration, even at NASA's lowest Reynolds number as shown in Fig. 9b. The UND data are overlaid (pink symbol) and show good agreement with the NASA data. Figure 9c shows the NASA high *Tu* baseline data along with the match point and three other sets of lower Reynolds number data from the UND facility. Even with the lower leading edge pressure tap resolution, the UND data show that the cove separation is apparent for Re_{Cx} < 0.2×Re_b.

With reasonable blade loading agreement shown at the match point conditions, further data can be examined highlighting the unique contributions of each of the facilities. Incidence angle effects at the lowest flow condition ($Re_{Cx,2}$ = 0.09×Re_b, $M_{2,i}$ = 0.72) are shown in Fig. 10 at high *Tu*. This condition is most applicable to the LCTR mission condition. The data show that the blade is highly loaded at the most positive incidence angle (i = +5.8°) due to high overall turning. As the incidence decreases, the blade loading and strength of the secondary flows are reduced. At i = −26.0° negative loading is observed on the front portion of the blade.

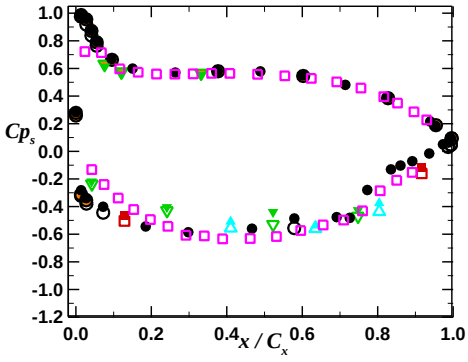

a.) 0.4×Re_b, $Ma_{2,i}$ = 0.72, Low *Tu*

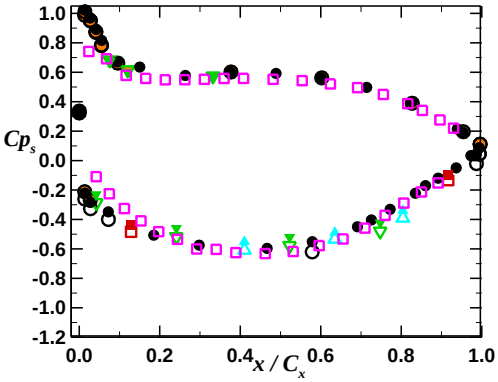

b.) 0.4×Re_b, $Ma_{2,i}$ = 0.72, High *Tu*

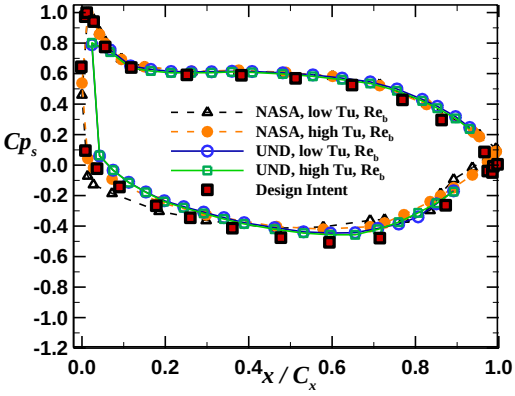

c.) Design Intent Loading

Figure 7. Facility Match Points at i = +5.8

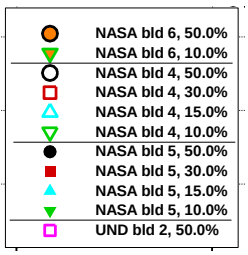

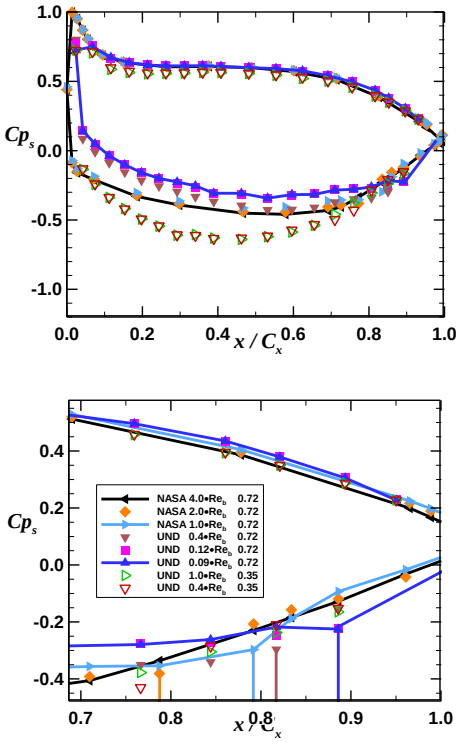

Figure 8. Effect of *Re* at *i* = +5.8, Low *Tu* (lines indicate region of flow reattachment).

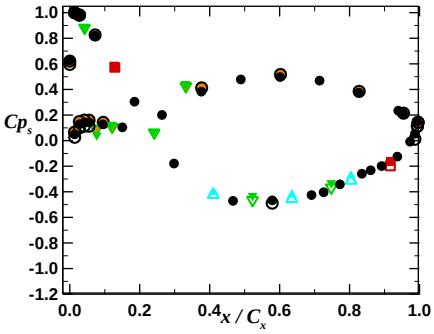

a.) NASA, 4.0×Re_b, $Ma_{2,i}$ = 0.72, Low *Tu*

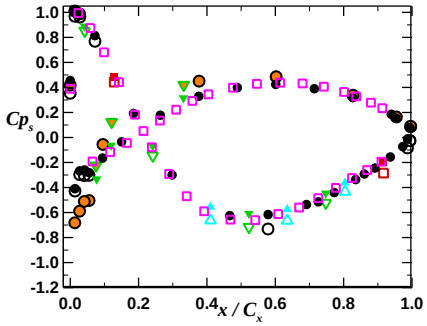

b.) NASA, 0.4×Re_b, $Ma_{2,i}$ = 0.35, High *Tu*, with UND match point

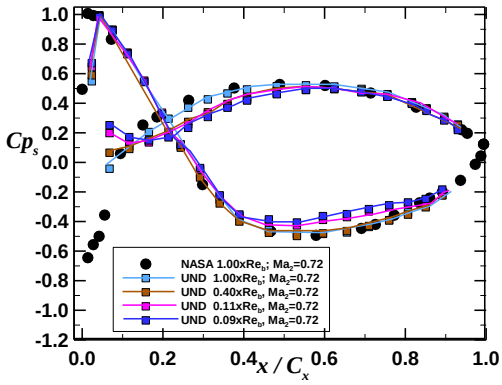

c.) NASA and UND: various *Re*, $Ma_{2,i}$ = 0.72, High *Tu*

Figure 9. Facility Match Points at *i* = −51.0°

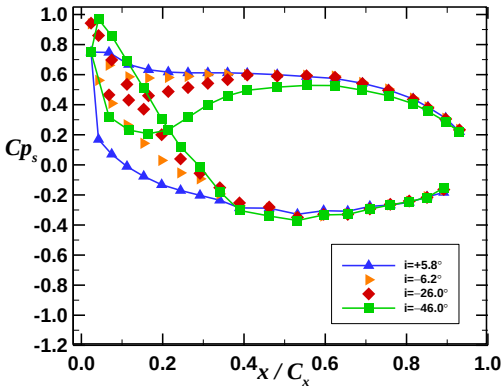

Figure 10. Effect of *i* at 0.09 x Re_b, $Ma_{i,2}$ = 0.72, High *Tu* in UND cascade.

Half-Span Flowfield Measurements

These datasets include half-span flowfield measurements for each flow condition. The NASA facility acquired detailed half-span surveys 7.0% axial chords downstream over three blade passages for two incidence angles at both high and low *Tu*.[8] Figure 11a illustrates the strong secondary flows observed at *i* = +5.8° at low inlet *Tu*. At this incidence angle, the blade is highly loaded, producing strong secondary flows

which transport thick endwall flow (e.g., 50% of the half-span) to and along the suction side of the blade. At high *Tu*, the turbulence grid established a thinner inlet boundary layer (~25% of span) which resulted in lower levels of aerodynamic blockage in the passage[8]. For the negative incidence case in Fig. 11b, the blade unloads and the flow becomes essentially two-dimensional.

The UND total pressure contours for the lowest Reynolds number ($0.09\times Re_b$) condition at the design exit Mach number are shown in Fig. 12 for i = +5.8° and i = −36.7°. Recall that the data from the two facilities cannot be overlaid directly because of differences in the probe survey measurement planes, the difference in aspect ratio of the cascades, and the difference in the relative boundary-layers thicknesses (aerodynamic blockage levels) in the two cascades. Figure 12a shows the influence of 95° of turning on the half-span exit losses at the +5.8° incidence angle. The strong passage vortex has swept the secondary low momentum fluid off of the endwall. This fluid has merged with the profile losses that includes the suction surface separation loss. The higher turbulence level in the present case has caused smoothing of the contours. The broad wake shown in Figure 12b at i = −36.7° is partially due to suction surface separation and partially due to the pressure side separation resulting from the highly negative inlet incidence angle. Additionally, the lower Reynolds number along with higher turbulence level also contributes to the higher loss levels. The typical upsweep of the endwall low momentum fluid with the passage vortex appears to be countered by the downward sweep of the pressure surface separation losses due to the cross-passage pressure gradient at this negative incidence angle. The lower *Tu* condition, presented by Long et al.[15], show similar behavior as indicated in Figs. 12a and 12b but with less smoothing.

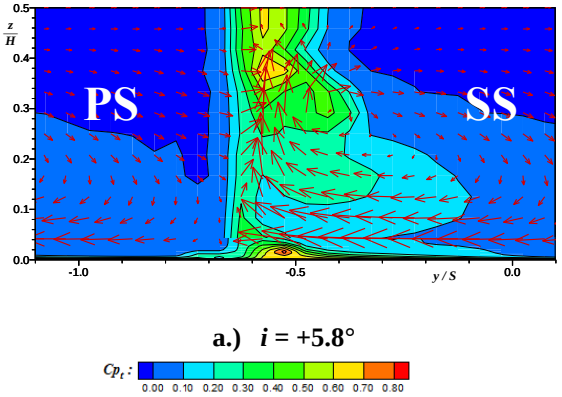

a.) i = +5.8°

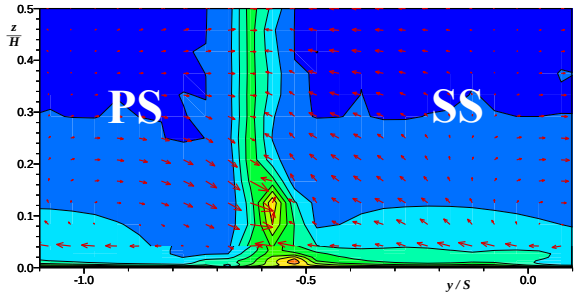

b.) i = −36.7°

Figure 11. Total-Pressure Contours with Velocity Vectors at Low *Tu*, Re_b, and $M_{2,i}$ = 0.72 (NASA).

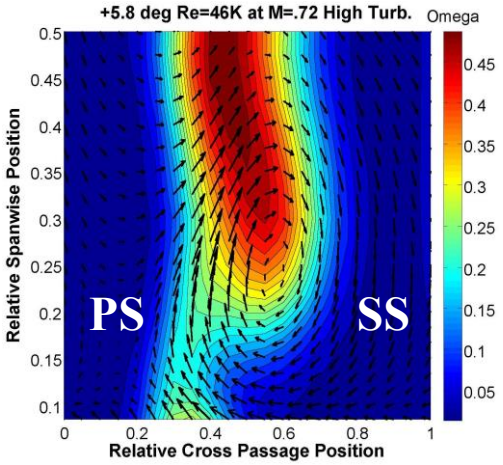

a.) i = +5.8°

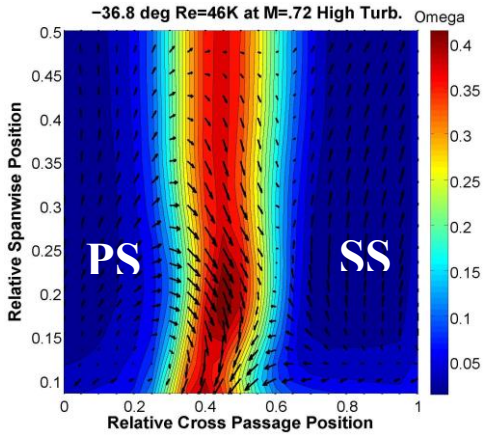

b.) i = −36.7°

Figure 12. Half-span Total-Pressure Contour with Velocity Vectors at high *Tu* (AC), 0.09× Re_b, and $M_{2,i}$ = 0.72 (UND).

Pitchwise Integrations

Pitchwise area-averaged (NASA) and cross-passage averaged (UND) integrations were calculated for each half-span flowfield measurement. The effects of turbulence intensity on the three-dimensional flow-field are shown in Figure 13. These data are calculated from the NASA dataset[7,8] at i = +5.8°, which show the largest secondary flow features. Figures 13a and 13b show a reduction in the area-averaged total-pressure coefficients along the blade span for high *Tu* (green lines). The core of the horseshoe vortex can be seen in Figs. 13c and 13d at z/H = 0.33 for low *Tu* and z/H = 0.24 for high *Tu*. This reflects that the thinner boundary layer, due to the upstream turbulence grid, causes the horseshoe vortex to be transported to a lower spanwise location on the blade.

Cross-passage averaged turning angle and total pressure losses (Ω) taken in UND's cascade are presented for high *Tu* (AC) in Figs. 14 and 15, showing the effects of Reynolds number and incidence. The averaged turning angle presented as a function of span in Fig. 14a is very consistent for the +5.8° incidence angle over the range of Reynolds numbers. The data show strong overturning near the wall due to a strong passage vortex. The data also show a mild under turning at z/H of between 0.3 and 0.36 due to the transport of the secondary loss core. The slightly higher midspan turning as compared to the NASA data of Fig. 13c is consistent with the slightly higher aft blade loading seen in Fig. 7c. The lower Mach number in Fig. 14a shows a reduced level of turning due to the shift in loading. The cross-passage averaged total pressure losses presented in Fig. 14b for the +5.8° incidence case show significant Reynolds number effects. The highest Reynolds number shows low losses in the near-wall region due to the action of the passage vortex. The loss peak due to the presence of the secondary loss core is clearly present at z/H = 0.36. The losses diminish toward midspan due to the attached suction surface boundary layer. However, at the lower Reynolds numbers the loss peak is not as discernable due to the higher suction surface separation losses which increase with decreasing Reynolds number.

The influence of incidence angle on cross-passage averaged turning is presented in Fig. 15a for an axial chord exit Reynolds number of 46,000 at the design exit Mach number. For the two highest incidence angles, i = +5.8° and i = −6.2°, significant overturning is present near the wall due to the action of the passage vortex. Incidence also has a significant influence on loss distribution as shown in Figure 15b. Generally, the decreasing incidence angle has a strong influence on the location of the secondary loss core off the surface of the endwall and the resulting cross-passage averaged loss distribution[15]. This loss distribution is also influenced by increasing separation loss on the pressure surface with decreasing incidence.

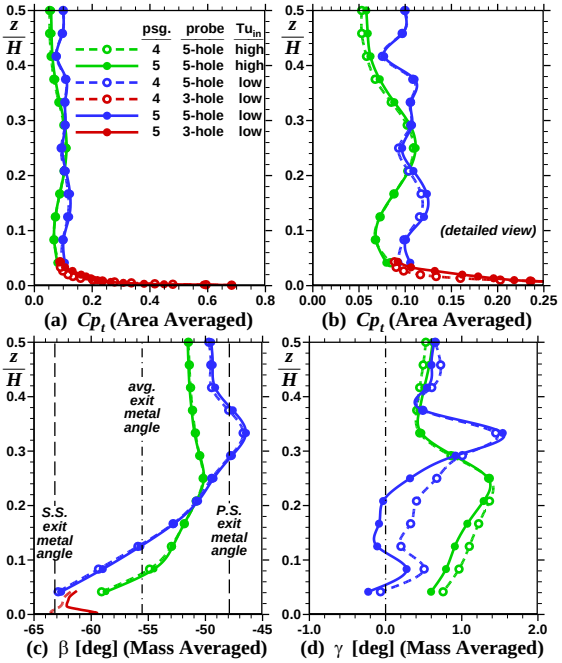

Figure 13. Pitchwise Integrations for i = +5.8°.

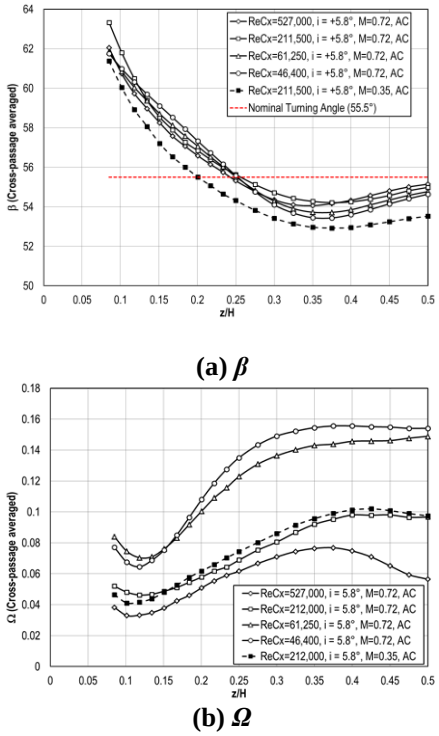

Figure 14. Reynolds number effects on Cross-passage averaged (a) turning angle and (b) total pressure losses, i = + 5.8°.

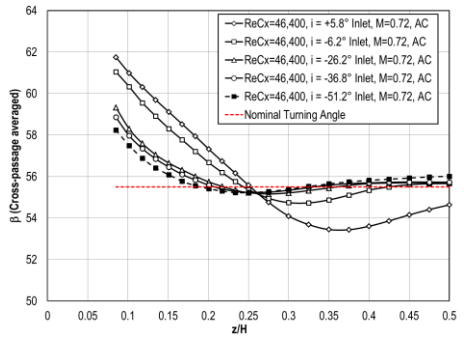

(a) *β*

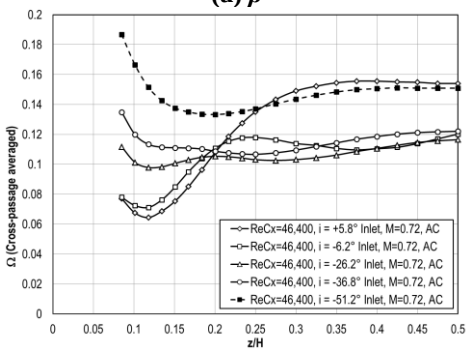

(b) *Ω*

Figure 15. Incidence effects on Cross-passage averaged (a) turning angle and (b) total pressure losses at Re_{Cx} = 46,000, $Ma_{2,i}$ = 0.72.

Stanton Number Distributions

Midspan heat transfer measurements were acquired on Blade 2 in UND's cascade to provide useful information on the state of the blade boundary layer. These data are presented in terms of Stanton number based on exit conditions in Figs. 16 and 17 for incidence angles of +5.8° and -36.8°. Figure 16 presents Stanton number distributions for the four Reynolds numbers including data for both exit Mach numbers at Re_{Cx} of 212,000 and 527,000 at the +5.8° incidence angles. At the M_2 = 0.72, an inflection point is present for the lower Reynolds numbers at an *s/C* of about 0.88 indicating a laminar separation. At the highest Reynolds number and for the two 0.35 exit Mach number cases transition is evident on the suction surface. On the pressure surface the heat transfer data suggest laminar flow over the surface for the two lowest Reynolds numbers but transition to turbulence is clearly present for the two highest Reynolds numbers at both Mach numbers. The $i = -36.8°$ results presented in Fig. 17 show similar results on the suction surface. However, on the pressure surface, clear evidence of separation and downstream reattachment is seen. The data suggest that the distance between the separation and reattachment points increases with decreasing Reynolds numbers.

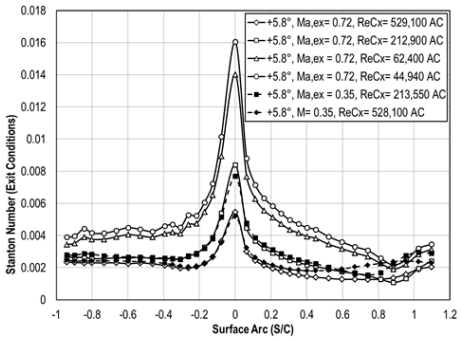

Figure 16. Influence of Re_{Cx} on Stanton number at high *Tu* (AC), *i* = +5.8°

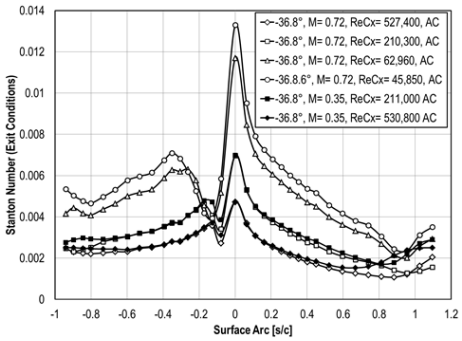

Figure 17. Influence of Re_{Cx} on Stanton number at high *Tu* (AC), *i* = −36.8°

Midspan Surveys

Mid-span total-pressure and exit flow angle surveys were acquired in both facilities over wide incidence ranges. It is important to note that the survey locations and traverse directions differ for both facilities and a direct overlay of the data cannot be made. However, key features of each dataset can be observed.

The effects of Reynolds number and exit Mach number from the UND facility are shown in Fig. 18 for i = +5.8° at low and high *Tu*. These data show that at low *Tu* (Fig. 18a) the suction side of the wake increases with decreasing Reynolds number. Similar trends due to Reynolds number can be seen even at high *Tu*. Figure 19 shows the NASA midspan total pressures for the highest negative incidence, i = –51.0°. At low inlet *Tu* (Fig. 19a), the pressure side separation spans across a majority of the passage and induces an aerodynamic blockage.[7] The wake depth and width increase significantly with decreasing Reynolds number. At the high inlet *Tu* (Fig 19b), the flow remains largely attached and a significant pressure-side separation is not seen except at the lowest Reynolds number. The wake thickness increases slightly on the pressure side with decreasing Reynolds number.

The corresponding UND i = –51.0° data are shown in Figure 20. Higher pressure side loss levels are seen for the two lowest Reynolds number cases, consistent with the blade loading observations discussed with Fig. 9c.

The effects of incidence on the midspan total-pressures are shown in Fig. 21 at the baseline Reynolds number (NASA) and Fig. 22 at the lowest Reynolds number conditions (UND). At the baseline Reynolds number (Fig. 21) the data are shown at low *Tu* where large separated flow effects can be observed. At the positive incidence angle (i = +15.8°) a strong suction side separation is evident. As the incidence decreases, the blade unloads and the losses decrease. At i = −36.7° the losses are at a minimum, however a pressure side loss increase can first be observed (McVetta et al.[7]). At the high negative incidence (i = −51.0°) the losses increase due to an extensive pressure-side separation. In Fig. 22 turbulence is introduced, however the UND data presented are at the lowest Reynolds number ($0.09\times Re_b$) condition at the design exit Mach number. The positive incidence angle shows high loss levels that decrease with decreasing incidence. Due to the turbulence, only a modest pressure side loss increase is observed at the highest negative incidence.

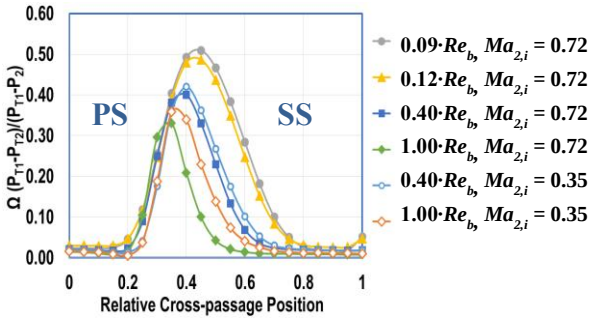

a) Low *Tu*

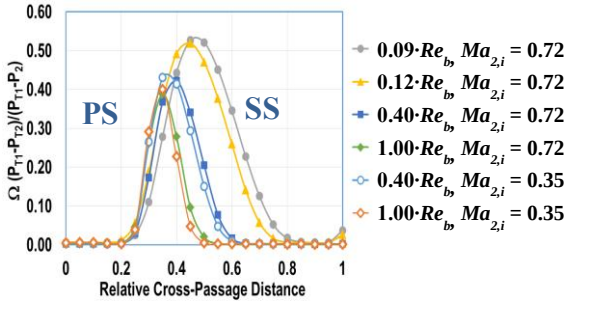

b.) High *Tu*

Figure 18. Effects of Reynolds Number and Exit Mach Number at i = +5.8°−UND.

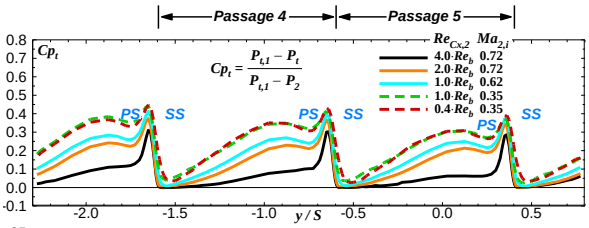

a) Low *Tu*

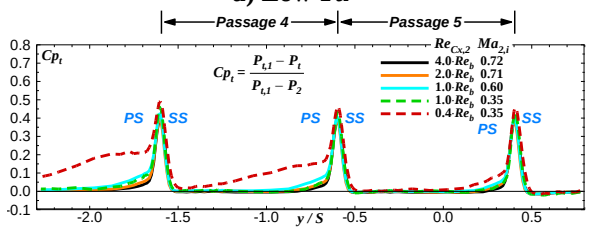

b) High *Tu*

Figure 19. Effects of Reynolds Number and Exit Mach Number at i = –51.0°−NASA.

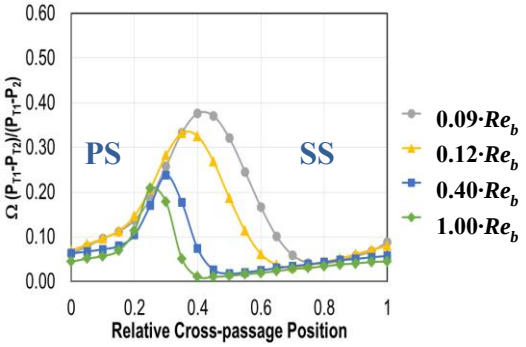

Figure 20. Effects of Reynolds Number at $Ma_{2,i}$ = 0.72, i = –51.0°, High *Tu*−UND.

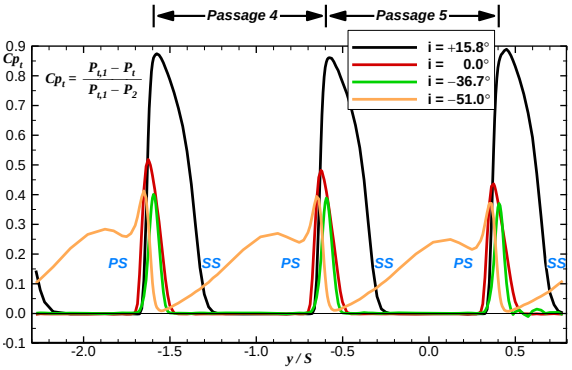

Figure 21. Effects of i at Re_b, $M_{2,i}$ = 0.72, Low *Tu*−NASA.

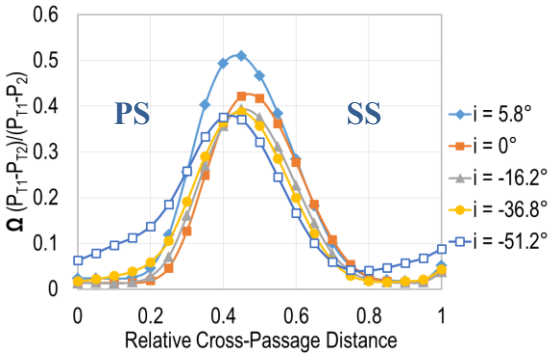

Figure 22. Effects of *i* at 0.09xRe_b, $M_{2,i}$ = 0.72, High *Tu*−UND.

Loss Buckets

Passage-average total-pressure loss is plotted as a function of incidence angle and Reynolds number in Figs. 23 from the UND facility (see Long et al.[15]). Figure 23a presents the losses at low *Tu* and shows a moderate level of losses at the higher two Reynolds numbers. However, the losses at the two lower Reynolds numbers are substantially higher (laminar scaling characteristic). The VSPT blade was designed to produce a compromise in efficiency between take off ($i = -36.7°$) conditions and high altitude cruise ($i = +5.8°$)[12]. This figure shows a reasonable balance between the loss levels at those conditions. At the lower Reynolds numbers, the increasingly negative incidence angles show increasing losses. The NASA passage averaged total-pressures at the Re_b match point is shown for $i = -36.7°$ and $i = +5.8°$. The two datasets show good agreement at these two incidence angles despite the differences in the inlet boundary layers.

For the high *Tu* case in Fig. 23b, the NASA and UND data vary however the trends are very similar. The losses for the UND dataset at the higher *Tu* condition are typically moderately higher than the lower turbulence case except at the high negative incidence angles where values are similar. Generally, these data show a significant increase in losses with decreasing Reynolds number due to laminar separation on the suction and pressure surfaces. However, the influence of the passing wakes and higher turbulence levels of actual engine conditions has the potential to reduce these separation losses due to their impact on transition.

Midspan profile loss coefficients, ω, were calculated from the NASA facility data for all ten incidence angles and five flow conditions[8] and are shown in Figure 24. The UND midspan passage losses at eight incidence angles and four flow conditions are overlaid on these plots. At low *Tu* in Fig. 24a the losses increase with decreasing Reynolds number. The UND and NASA Re_b match point data (cyan) show very similar trends despite the different measurement planes. However, due to the thick inlet boundary layer the NASA losses at this point tend to be higher.

In Fig. 24b the midspan loss is shown for high *Tu*. As previously mentioned, NASA tested at much higher inlet turbulence intensities (*Tu* = 8%-15%). The NASA data show that sensitivity of loss levels to Reynolds number at high *Tu* is greatly reduced and the losses collapse asymptotically to the high Reynolds number (turbulent) level. It was found that by applying a power law scaling ($\omega \propto Re^{-n}$) to the midspan loss data, the low *Tu* midspan losses are dominated by laminar flow and the high *Tu* are influenced by turbulent flow[8].

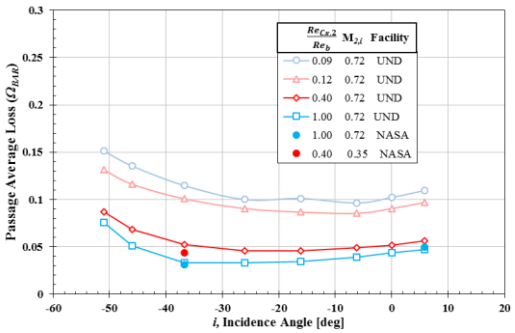

a.) Low *Tu* (LT)

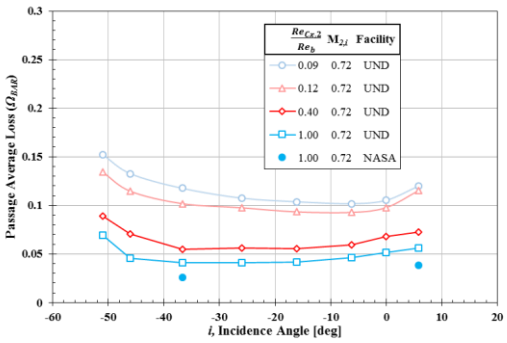

b.) High *Tu* (AC)

Figure 23. Total passage average loss (Ω_{BAR}) vs. incidence angle at various Re_{Cx}.

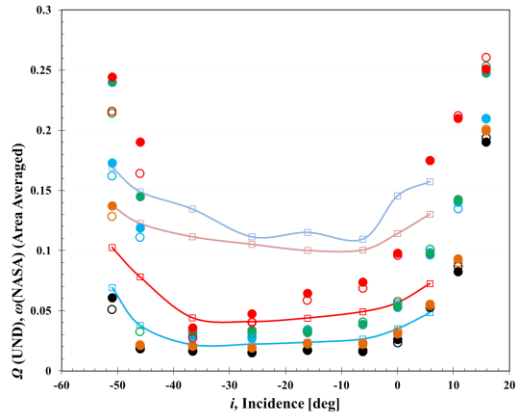

a) Low *Tu*

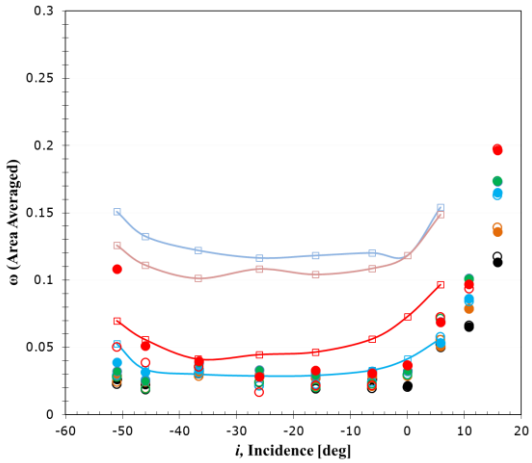

b) High *Tu*

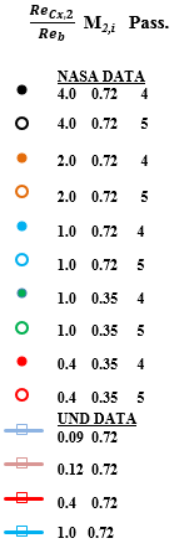

Figure 24. Midspan Loss vs. Incidence.

Conclusions

A summary of the complementary aerodynamic performance datasets for a VSPT blade section were presented in this paper. Detailed measurements were acquired in the NASA Transonic Turbine Blade Cascade Facility and the University of North Dakota High Speed Compressible Flow Wind Tunnel Facility. The data were obtained over a large range of Reynolds numbers, Mach numbers, incidence angles, and inlet turbulence intensities. The NASA facility has the ability to test over a high range of Reynolds numbers and the UND facility complemented the dataset by testing at lower Reynolds numbers at the design exit Mach number and by acquiring heat transfer measurements. This expanded dataset allows for validation of transition models and helps inform designers to advance future VSPT concepts.

Observations provided have highlighted the impact of relative boundary-layer thicknesses, Reynolds number and inlet turbulence levels, Mach number, and incidence on blade row loading loss, and turning levels, boundary-layer state, and exit flow field characteristics.

Acknowledgements

This work was supported under the NASA Advanced Air Vehicle Program, Revolutionary Vertical Lift Technology Project. The NASA authors would like to acknowledge Doug Thurman (Army Research Laboratory) for his assistance during the NASA cascade testing. The measurements acquired at the University of North Dakota and documented in this paper were supported through NASA CAN funding (Grant No. NNX11AQ32A), Jeppie Compton program manager. The North Dakota NASA EPSCoR program also supported the design and fabrication of the current blade cascade. The authors also thank Adam Ford, Matt Bloxham, Steve Gegg (deceased), and Ed Turner of Rolls-Royce North American Technologies for their contributions during the blade design efforts under the NASA RTAPS contract.

References

1. Wilkerson, J. B. and Smith, R. L., "Aircraft System Analysis of Technology Benefits to Civil Transport Rotorcraft," NASA/CR—2009–214594, June, 2009.
2. *Clean Sky 2 Joint Undertaking Work Plan 2014-2015*, CS-GB-2014-03-07, 2014.
3. Warwick, G., "Army Protects Funding For Advanced Rotorcraft," *Aviation Week & Space Technology*, Mar., 2013.

4. Acree, C. W., Hyeonsoo, Y., and Sinsay, J. D., "Performance Optimization of the NASA Large Civil Tiltrotor," *Proc. Int. Powered Lift Conf.*, London, UK, July, 2008.
5. Welch, G. E., "Assessment of Aerodynamic Challenges of a Variable-Speed Power Turbine for Large Civil Tilt-Rotor Application," *Proc. AHS Int. 66th Ann. Forum*, Phoenix, AZ, May, 2010; also NASA/TM—2010–216758, Aug. 2010.
6. Welch, G. E., McVetta, A. B., Stevens, M. A., Howard, S. A., Giel, P. W., Ameri, A. A., To, W-M., Skoch, G. J., Thurman, D. R., "Variable-Speed Power-Turbine Research at Glenn Research Center," *Proc. AHS Int. 68th Annual Forum*, Ft. Worth, TX, May, 2012.
7. McVetta, A. B., Giel, P. W., and Welch, G. E., " Aerodynamic Measurements of A Variable-Speed Power-Turbine Blade Section in a Transonic Turbine Cascade At Low Inlet Turbulence," ASME/GT2013-94695, Jun, 2013; also NASA/TM—2013-218069, Aug, 2013.
8. Flegel, A. B., Giel, P. W., and Welch, G. E., "Aerodynamic Effects of High Turbulence Intensity on a Variable-Speed Power-Turbine Blade with Large Incidence and Reynolds Number Variations," AIAA-2014-3933, Proc. 50th Joint Propulsion Conference, Jul, 2014. Also NASA/TM-2014-218137.
9. Ameri, A. A., Use of Transition Modeling to Enable the Computation of Losses for Variable-Speed Power Turbine, ASME GT2012-69591, Jun 2012.
10. Ameri, A., Giel, P. W., McVetta, A. B., "Validation of a CFD Methodology for Variable Speed Power Turbine Relevant Conditions," GT2013-95030, ASME Turbo Expo., San Antonio, Texas, USA, June 2013.
11. Ameri, A., Giel, P. W., Flegel, A. B., 2014, "Simulation of VSPT Experimental Cascade under High and Low Free-Stream Turbulence Conditions," AIAA-2014-3935, 50th Joint Propulsion Conference, Cleveland, Ohio, July 2014. Also NASA/TM-2015-218457.
12. Ford, A., Bloxham, M., Turner, E., Clemens, E., Gegg, S., "Design Optimization of Incidence-Tolerant Blading Relevant to Large Civil Tilt-Rotor Power Turbine Applications," NASA/CR—2012-217016, Dec. 2012.
13. Mihelish, M. and Ames, F.E., 2013, "The development of a closed loop high speed cascade wind tunnel for cascade testing at moderate to low Reynolds numbers, ASME/GT2013-95048, 2013.
14. Moualeu, L. P. G., Long, J. A., Stahl, K. A., Ames, F. E., and Suzen, Y. B., "Midline Heat Transfer and Pressure Measurements on an Incident Tolerant Blade Section for a Variable Speed Power Turbine at Low to Moderate Reynolds Numbers in a Transonic Turbine Cascade," AIAA-2014-3936, *Proc. 50th Joint Propulsion Conference*, Jul 2014.
15. Long, J.A, Moualeu, L.P.G., Hemming, N.J., Ames, F.E., Suzen, Y.B., "Variable Speed Power Turbine Measurements at Low to Moderate Reynolds Numbers in a Transonic Turbine Cascade: Aerodynamic Loss Surveys", GT2015-42504, ASME Turbo Expo, Montreal, Canada, June 2015.
16. Verhoff, V. G., Camperchioli, W. P, and Lopez, I., 1992, "Transonic Turbine Blade Cascade Testing Facility", AIAA Paper No. 92-4034, NASA TM-105646.
17. Giel, P.W., Sirbaugh, J.R, Lopez, I., and Van Fossen, G. J., 1996b, "Three Dimensional Navier Stokes Analysis and Redesign of an Imbedded Bellmouth Nozzle in a Turbine Cascade Inlet Section," ASME Journal of Turbomachinery, 118, No 3, pp 529-535. NASA/TM-107284 and U.S. Army ARL-MR-152.
18. Thurman, A., Giel, P. W., Flegel, A. B., "Inlet Turbulence and Length Scale Measurements in a Large Scale Transonic Turbine Cascade," AIAA-2014-3934, *Proc. 50th Joint Propulsion Conference*, Cleveland, Ohio, July 2014.